


# Measurement of vertebral bone marrow proton density fat fraction in children using quantitative water–fat MRI

Stefan Ruschke<sup>1</sup>  · Amber Pokorney<sup>2</sup> · Thomas Baum<sup>1,3</sup> · Holger Eggers<sup>4</sup> · Jeffrey H. Miller<sup>2</sup> · Houchun H. Hu<sup>2</sup> · Dimitrios C. Karampinos<sup>1</sup>

Received: 12 January 2017 / Revised: 23 March 2017 / Accepted: 24 March 2017 / Published online: 5 April 2017  
© ESMRMB 2017

## Abstract

**Objectives** To investigate the feasibility of employing a 3D time-interleaved multi-echo gradient-echo (TIMGRE) sequence to measure the proton density fat fraction (PDFF) in the vertebral bone marrow (VBM) of children and to examine cross-sectional changes with age and intra-individual variations from the lumbar to the cervical region in the first two decades of life.

**Materials and methods** Quantitative water–fat imaging of the spine was performed in 93 patients (49 girls; 44 boys; age median 4.5 years; range 0.1–17.6 years). For data acquisition, a six-echo 3D TIMGRE sequence was used with phase correction and complex-based water–fat separation. Additionally, single-voxel MR spectroscopy (MRS) was performed in the L4 vertebrae of 37 patients. VBM was manually segmented in the midsagittal slice of each vertebra. Univariable and multivariable linear regression models were calculated between averaged lumbar, thoracic and cervical bone marrow PDFF and age with adjustments for sex, height, weight, and body mass index percentile.

**Results** Measured VBM PDFF correlated strongly between imaging and MRS ( $R^2 = 0.92$ , slope = 0.94,

intercept =  $-0.72\%$ ). Lumbar, thoracic and cervical VBM PDFF correlated significantly (all  $p < 0.001$ ) with the natural logarithm of age. Differences between female and male patients were not significant ( $p > 0.05$ ).

**Conclusion** VBM development in children showed a sex-independent cross-sectional increase of PDFF correlating with the natural logarithm of age and an intra-individual decrease of PDFF from the lumbar to the cervical region in all age groups. The present results demonstrate the feasibility of using a 3D TIMGRE sequence for PDFF assessment in VBM of children.

**Keywords** Bone marrow · Child · Magnetic resonance imaging · Proton density fat fraction · Water–fat imaging · Chemical shift-encoding based imaging

## Introduction

Bone marrow is traditionally described by the manifestation of two compartments, which can be distinguished by their histogenesis and are called red bone marrow or yellow

✉ Stefan Ruschke  
stefan.ruschke@tum.de

Amber Pokorney  
apokorney@phoenixchildrens.com

Thomas Baum  
thomas.baum@tum.de

Holger Eggers  
holger.eggert@philips.com

Jeffrey H. Miller  
jhmiller@phoenixchildrens.com

Houchun H. Hu  
harryhhu@gmail.com

Dimitrios C. Karampinos  
dimitrios.karampinos@tum.de

<sup>1</sup> Department of Radiology, Klinikum rechts der Isar, Technical University of Munich, Ismaninger Straße 22, 81675 München, Germany

<sup>2</sup> Radiology, Phoenix Children's Hospital, 1919 E Thomas Rd, Phoenix 85016, AZ, USA

<sup>3</sup> Department of Diagnostic and Interventional Neuroradiology, Klinikum rechts der Isar, Technical University of Munich, Ismaninger Straße 22, 81675 München, Germany

<sup>4</sup> Philips Research Laboratory, Röntgenstraße 24-26, 22335 Hamburg, Germany

bone marrow, depending upon the predominance of hematopoietic or fatty tissue, respectively [1]. Its normal physiology appears as a gradual conversion of hematopoietic marrow to fatty marrow showing skeletal site, age and sex specific characteristics [2, 3]. Based on the intrinsically different response to hematopoietic demands [4], Scheller et al. [5] recently proposed to differentiate bone marrow adipocytes interspersed with active hematopoiesis, referred to as regulated marrow adipose tissue (MAT), from those occurring in other regions that are preserved, i.e. constitutive MAT [6].

Proton density fat fraction (PDFF) is an MR-based parameter that has been primarily used to assess the presence of hematopoietic and fatty marrow. It has been recently shown that PDFF correlates with bone marrow cellularity [7–9]. Therefore, there has been an increasing interest in using single-voxel MR spectroscopy (MRS) [10–16] and imaging [13, 17–19] to quantify PDFF in vertebral bone marrow (VBM). The quantitative assessment of PDFF has been used in multiple clinical applications, including the characterization of bone health [18, 20–22], metabolic disorders [23–25], and cancer [26, 27]. Its usefulness has been demonstrated in monitoring the physiological status of bone marrow and its post-therapeutic patterns after radiation and chemotherapy-based cancer treatments [28–31], the estimation of radiation doses applied to active bone marrow based on its quantitative distribution [32] and as a complement to biopsies by extracting additional information supporting the diagnosis, staging, and follow-up of hematologic malignancies [33].

Chemical shift-encoding based water–fat imaging techniques have the advantage of enabling spatially resolved PDFF maps, allowing the probing of multiple vertebrae in a single measurement compared to single-voxel spectroscopy. Numerous confounding factors have to be considered in PDFF quantification including the B<sub>0</sub> field inhomogeneity [34, 35], the T<sub>2</sub>\* decay [36, 37], the multi-frequency appearance of the fat signal [37, 38], the T<sub>1</sub> difference between water and fat components [39, 40], any temperature- or susceptibility-induced fat resonance frequency shifts [41, 42], the concomitant gradient field [43, 44], noise bias [39], and phase errors [44–49].

The majority of the existing work measuring VBM PDFF has focused on adults and the elder population and data in children, in particular normative data, remain limited. In adults, the bone marrow fat fraction has been negatively associated with trabecular bone density, raising interest about its functional significance and implications for skeletal integrity [50]. In children, a better understanding of the bone development process at an early age [51] may gain insight into potential effects on adverse bone health throughout later life. Hence, a robust and accurate assessment of VBM PDFF in children may improve our

understanding of VBM development and may help identifying deviations from normal physiology. In addition, imaging of pediatric patients usually requires smaller voxel sizes compared to adults, which leads to an increased echo time step in multi-echo gradient-echo based water–fat imaging and therefore decreases the performance of the water–fat separation process [52]. As previously demonstrated, a time-interleaved multi-echo gradient-echo (TIMGRE) water–fat pulse sequence [44] enables robust water–fat decomposition by allowing a flexible selection of echo times independently of voxel size by interleaving echoes in several repetition times (TRs).

The purpose of the present study was (a) to investigate the feasibility of employing a 3D TIMGRE sequence to measure PDFF in the VBM of children, (b) to examine cross-sectional changes with age and (c) to examine intra-individual PDFF variations from the lumbar to the cervical region in the first two decades of life.

## Materials and methods

### Study design

The present study prospectively enrolled and acquired data from 109 patients. All subjects were scheduled to receive routine spine MRI examinations for clinically indicated reasons at our institution. General anesthesia was administered in all cases. The decision to use anesthesia in each patient was not a part of the present research study. The decision was made under a separate clinical setting by the patient, his/her parents or legal guardians, and an attending anesthesiologist. None of the authors of this study were involved in the decision to use anesthesia. The addition of the TIMGRE pulse sequence and single-voxel MRS was approved by the institutional review board. Informed consent was obtained and the study was HIPAA-compliant (Health Insurance Portability and Accountability Act).

All measurements were performed with two identical 3T Ingenia MRI scanners (Philips Healthcare, Best, the Netherlands) using the built-in 12-channel posterior table coil array for signal reception.

### Subjects

Of the 109 recruited subjects, a cohort of 93 subjects (median age = 4.5 years), including 49 female (median age = 5.4 years) and 44 male (median age = 3.6 years) patients, was included in the final data analysis. Sixteen cases [chemotherapy (1), radiation therapy (1), myelomeningocele (1), partial intervertebral osseous fusion and disc space narrowing (1), diffuse fatty marrow signal and tumor in the pineal region (1), dorsal myelomeningocele

repair (1), wedge deformity with a sharp kyphosis and edema (1), data not acquired (5), incomplete raw data (3), motion artifacts (1)] were excluded after a pediatric neuroradiologist reviewed the patient's medical history and the corresponding images and noted the presence of VBM and spine pathologies that might impact (or confound) VBM PDFF measurements. The cohort characteristics are summarized in Table 1. There were no significant differences between the female and male cohort considering age ( $p = 0.160$ ), height ( $p = 0.192$ ), weight ( $p = 0.179$ ), BMI ( $p = 0.659$ ) and BMI percentile ( $p = 0.501$ ).

### Single-voxel spectroscopy

For validation, the L4 vertebrae of 37 subjects was measured using a single-voxel (SV) stimulated-echo acquisition mode (STEAM) MR spectroscopy sequence with dynamic TE values. The voxel was placed to lie completely within the trabecular bone compartment, and had typically a size around  $10 \times 10 \times 10 \text{ mm}^3$ . Chemical shift displacement between fat and water was taken into consideration by making sure that the water-excited and fat-selective voxels laid within the bone marrow compartment. Other parameters included: spectral bandwidth = 3000 Hz; RF pulse bandwidth = 2277 Hz (inducing a chemical shift displacement error of 19.3% of the MRS voxel size); TE = 12/16/20/24 ms; TM = 18 ms; TR = 5000 ms; number of signal averages = 4; number of phase cycles = 4; total scan time = 2:05 min. PDFF was then estimated using an in-house built frequency-domain-based peak-fitting routine doing a joint fitting over the acquired TEs with constrained peak amplitudes according to the VBM triglyceride structure above (as previously performed in [16]).

### Quantitative water–fat imaging

The TIMGRE sequence used in this work for quantitative chemical shift-encoded water–fat imaging employed an acquisition scheme that consisted of two interleaved TRs acquiring three echoes, each using fly-back gradients

with constant effective echo time spacing. Typical imaging parameters used in this study were: 16–26 sagittal slices with a slice thickness of 1.2–3 mm; S/I and A/P FOV = 360–500 and 140–240 mm; in-plane voxel resolution = 1.2–1.6 mm; no sensitivity encoding acceleration (SENSE); no partial Fourier sampling; flip angle = 3 degrees (to reduce T1-bias [40]); TR = 8.8–12.9 ms; effective TE spacing = 1.2–1.3 ms; first TE = 1.5–1.7 ms; total scan time = 2–3 min. In the case of taller subjects, the FOV was split in the FH direction in 2 stacks to cover the whole spine.

The water–fat separation routine used to determine PDFF was based on a complex-based multi-peak water–fat signal model with single T2\* correction [37, 38], which is essential in the presence of trabecular bone [19, 53]. PDFF was calculated using the magnitude discrimination approach [39]. Phase errors arising from echo misalignments, the concomitant gradient field and a constant phase offset between interleaves were corrected in order to enable a robust water–fat separation [44]; the initial fieldmap estimation was done using Berglund et al.'s [54] multi-seed region growing approach from the ISMRM water–fat toolbox [55]. The fat model was calibrated according to the previously reported vertebral bone marrow triglyceride structure [16, 56, 57] with *ndb* (mean number of double bounds per triglyceride) = 3.13, *nmldb* (mean number of methylene-interrupted double bounds per triglyceride) = 0.7, and *CL* (mean fatty acid chain length) = 17.3.

### Water–fat imaging analysis

Regions of interests (ROIs) were manually drawn in the midsagittal slice of the bone marrow compartment for each vertebra in the magnitude images and then transferred to the PDFF maps and exported using the Software OsiriX (Pixmeo, Bernex, Switzerland) and Horos (The Horos Project, [www.horosproject.org](http://www.horosproject.org)). Reproducibility of these measurements has been reported previously with

**Table 1** Study cohort characteristics

	All subjects	Female	Male	<i>p</i> value
<i>n</i>	93	49	44	
Age (years)	4.5 (0.1–17.6)	5.4 (0.1–17.6)	3.6 (0.2–15.8)	0.160
Height (cm)	104.4 (49.2–165.0)	113.4 (49.2–164.3)	99.3 (57.6–165.0)	0.192
Weight (kg)	17.6 (3.1–78.9)	19.3 (3.1–67.0)	16.6 (5.3–78.9)	0.179
BMI	16.8 (12.9–30.0)	16.7 (12.9–30.0)	16.9 (13.9–29.0)	0.659
BMI percentile	61.0 (0.0–100.0)	58.5 (0.0–100.0)	61.5 (0.0–100.0)	0.501

Median (min.–max.) age, height, weight, body mass index (BMI), and BMI percentile of the cohort. The *p* values were determined between female and male sub-cohorts using a nonparametric Mann–Whitney *U* test and a *z*-statistic approximation. *n* number of subjects

an absolute precision error of 1.7% averaged over C3–L5 [17].

### Statistical analysis

Mann–Whitney  $U$  test was performed between female and male study subjects for age, height, weight, BMI, and BMI percentile. Correlation, Bland–Altman analysis and a two-tailed paired  $t$  test were performed for measuring bone marrow PDFF in the L4 vertebrae between quantitative water–fat imaging and MRS.

Univariable and multivariable linear regression models were calculated between measured PDFF averaged for lumbar (L5–L1), thoracic (T12–T1), and cervical (C7–C3) vertebrae groups as dependent variable, and the natural logarithm ( $\ln()$ ) of age as independent variable adjusted for sex, height, weight, and BMI percentile with a 0.05 level of significance.  $\ln(\text{age})$  was an ad hoc choice and used due to the visual appearance of the correlation curve between PDFF and age and its beneficial properties in statistical analysis.

Patients were grouped into six groups for further statistical analysis from 0–0.4, 0.5–1.4, 1.5–2, 3–4, 5–8, and 9–18 years, respectively. Mean  $\pm$  standard deviation (SD) PDFF was calculated for each age group: lumbar (L5–L1), thoracic (T12–T1) and cervical (C7–C3) vertebrae groups in all subjects, in the female subjects and in the male subjects, respectively. Homoscedastic two-sampled  $t$  tests were performed for female and male subjects in the same age group and vertebral location. A logarithmic fit ( $y = a + b * \ln(x)$ ) along with its coefficient of determination  $R^2$  was performed for vertebral bone marrow PDFF grouped by vertebral group as a function of age.

The L3 vertebral body was selected as a representative vertebral level (as previously reported in [58, 59]) to perform an age and sex comparison. Mean  $\pm$  SD PDFF was also calculated for each age group for the L3 vertebrae in all the subjects, in the female subjects and in the male subjects, respectively. Nonparametric Mann–Whitney  $U$  tests were performed for female and male subjects in the same age group.

Statistical processing was performed in Excel for Mac Version 15.26 (Microsoft, Redmond, WA) for the correlation, Bland–Altman analysis and  $t$  test comparing quantitative water–fat imaging and spectroscopy; in SPSS version 17.0 (SPSS Institute, Chicago, IL, USA) for the univariable and multivariable linear regression models and in MATLAB R2015b & R2016a (Mathworks, Natick, MA, USA) for all other measures. All statistical tests were performed with a 0.05 level of significance.

### Results

#### Quantitative water–fat imaging versus single-voxel spectroscopy PDFF

Single-voxel spectroscopy was obtained in the L4 vertebra (L3 was measured in cases where it could not be performed in L4) in 37 of the recruited patients. Linear correlation of the agreement of VBM PDFF measurement by imaging and spectroscopy in the L4 vertebra yielded an intercept of  $-0.72$  [95% confidence interval (CI)  $(-4.00, 2.56)$ ] and slope of  $0.94$  [95% CI  $(0.85, 1.03)$ ] with  $R^2 = 0.92$ ;  $p < 0.001$ . (Figure 1a) A  $t$  test showed that slope and intercept do not significantly differ from 1 ( $p = 0.193$ ) and 0 ( $p = 0.661$ ), respectively. The

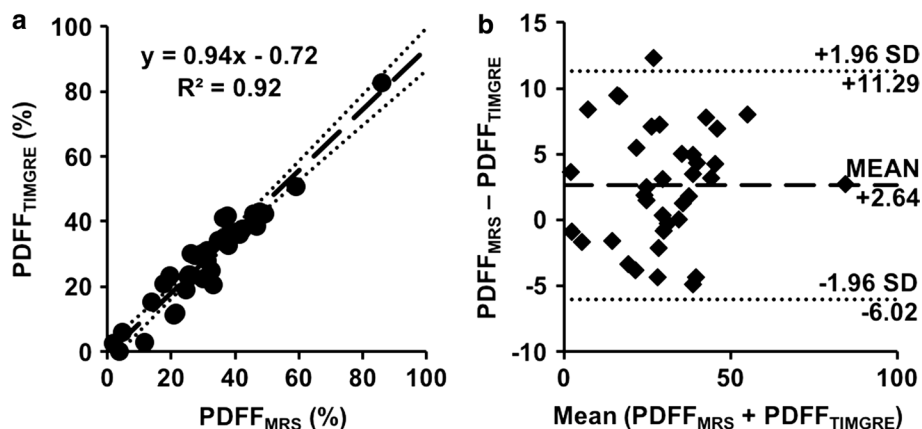


**Fig. 1** **a** Correlation plot of measured PDFF (%) in the L4 vertebrae of 37 patients using a single-voxel MRS and TIMGRE-based approach. *Dotted lines* represent lower and upper 95% CI, *dashed line* represents linear correlation, respectively. **b** Bland–Altman for

the same entities as in (a). *Dotted lines* represent the mean  $\pm$  1.96 SD, *dashed line* represents the mean, respectively. PDFF proton density fat fraction, CI confidence interval, SD standard deviation

Bland–Altman analysis showed a mean difference of 2.64 with limits of agreement ( $\pm 1.96$  SD) of 11.29 and  $-6.02$  (Fig. 1b).

### Imaging PDFF maps

Figure 2 shows representative PDFF maps in patients with increasing age, i.e. from a 0.4-year-old male to a 6.4-year-old female: PDFF maps show a decreased VBM PDFF from the lumbar to the cervical region within the same subject and cross-sectionally with age as well.

### VBM PDFF dependence on age

Results from the univariable and multivariable linear regression models are summarized and tabulated in Table 2. Multivariable linear regression models between measured average lumbar (L5–L1), thoracic (T12–T1) and cervical (C7–C3) bone marrow PDFF and  $\ln(\text{age})$ , adjusted for sex, height, weight, and BMI percentile yielded a significant correlation for  $\ln(\text{age})$  versus the lumbar ( $p < 0.001$ ), thoracic ( $p < 0.001$ ), and cervical region ( $p = 0.033$ ). Adjusted parameters did not reach statistical significance ( $p > 0.05$ ).

The univariable linear regression models tabulated in Table 2 also showed a significant correlation for the measured mean lumbar ( $p < 0.001$ ), thoracic ( $p < 0.001$ ), and cervical ( $p < 0.001$ ) bone marrow PDFF with the  $\ln(\text{age})$ . Figure 3 shows, in analogy to Table 2, the measured average lumbar, thoracic, and cervical bone marrow PDFF as a function of age, with  $R^2$  values of 0.552, 0.567, and 0.338, respectively.

### VBM PDFF dependence on spinal location

Table 3 summarizes the measured differences in average lumbar, thoracic and cervical bone marrow PDFF between female and male subjects, which were not significant ( $p > 0.05$ ) in any age group. Figure 4 displays, complementary to Table 3, the measured VBM as a function of spinal location for the defined age groups, showing a decreasing PDFF from the lumbar to the cervical region for all age groups. VBM PDFF as function of vertebral location yielded linear correlations with a decreasing slope ranging from  $-0.3$  to  $-1.0$  and intercept ranging from 3.1 to 37.6% from younger towards older age groups, respectively.

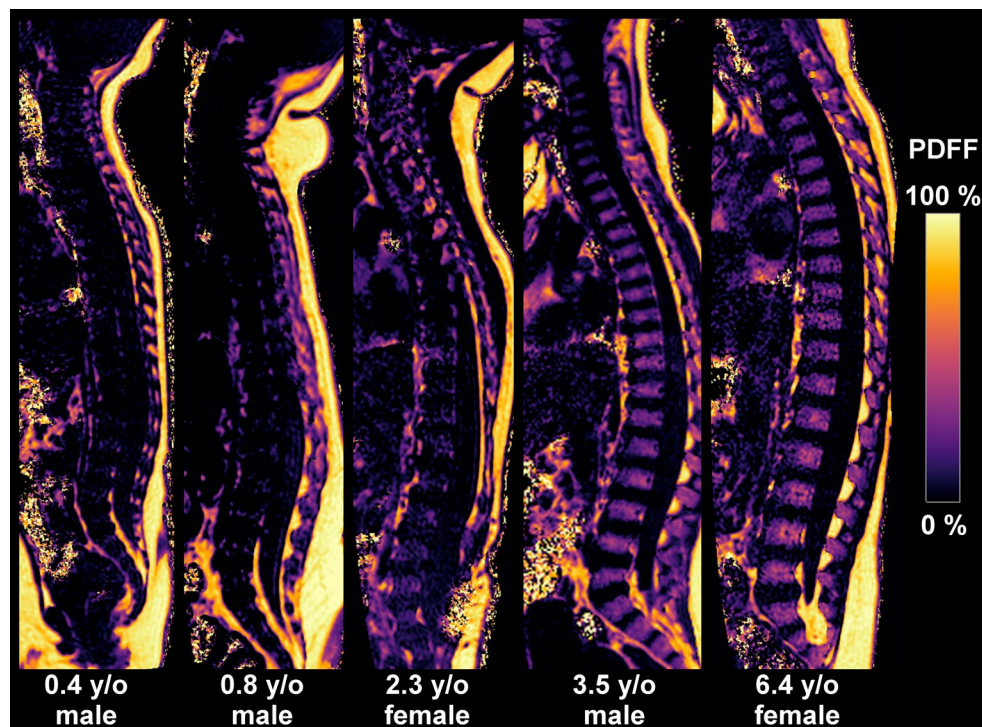


**Fig. 2** Five representative full spine PDFF maps picked from the five youngest age groups showing a 0.4-year-old male, 0.8-year-old male, 2.3-year-old female, 3.5-year-old female, and 6.4-year-old female, respectively. Note the increase in PDFF over age and from cervical to lumbar spine. PDFF in the under-1-year-olds is nearly indistinguishable

from 0%. In the 2.3-year-old the outlines of the L-spine and lower T-spine vertebrae start becoming visible in the PDFF map, whereas the upper T-spine and C-spine vertebrae still show a low PDFF. PDFF proton density fat fraction, % year-old

**Table 2** Statistical analysis: univariable and multivariable linear regression models

	Univariable linear regression			Multivariable linear regression adjusted for sex, height, weight, BMI percentile		
	$\beta$	$p$ value	95% CI	$\beta$	$p$ value	95% CI
Average L5–L1						
Intercept	14.16	<0.001	(11.42, 16.89)	25.01	0.029	(2.69, 47.34)
Ln(age)	8.66	<0.001	(7.03, 10.28)	12.65	<0.001	(7.74, 17.56)
Average T12–T1						
Intercept	8.59	<0.001	(6.13, 11.04)	10.59	0.312	(–10.10, 31.28)
Ln(age)	8.01	<0.001	(6.55, 9.47)	9.20	<0.001	(4.65, 13.75)
Average C7–C3						
Intercept	3.81	0.006	(1.14, 6.48)	10.62	0.528	(–22.83, 44.07)
Ln(age)	5.32	<0.001	(3.49, 7.15)	6.29	0.033	(0.51, 12.07)

Correlation coefficients  $\beta$ ; 95% confidence interval (CI) lower (LB) and upper (UB) bounds; and  $p$  values from univariable and multivariable linear regression models for measured PDFF averaged for L5–L1, T12–T1, and C7–C3 for the variables Ln(age) (natural logarithm of age), sex, height, weight, and BMI percentile

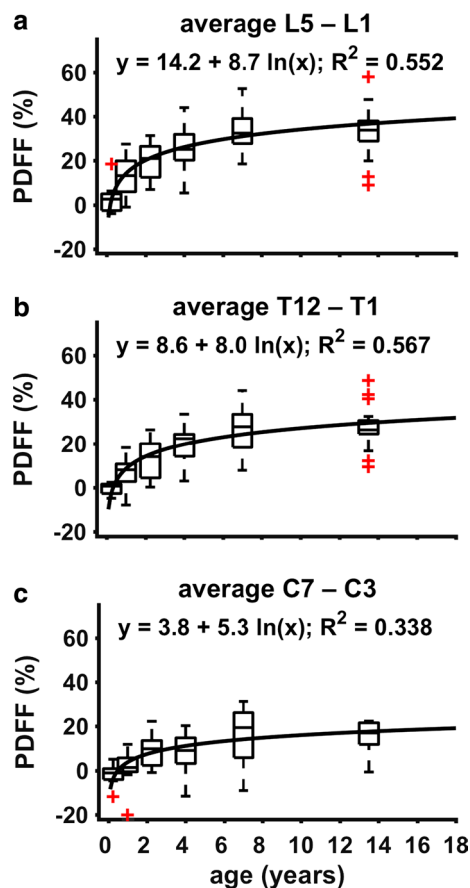


**Fig. 3** Boxplot of measured mean VBM PDFF in the **a** lumbar, **b** thoracic and **c** cervical spine for age groups 0–0.4, 0.5–1.4, 1.5–2, 3–4, 5–8, and 9–18 years, respectively. The equations the fitted logarithmic function ( $y = a + b \times \ln(x)$ ) and  $R^2$  are given for the three spinal regions. Outliers are indicated by red crosses. VBM vertebral bone marrow, PDFF proton density fat fraction

### Meta-analysis on L3 bone marrow fat fraction dependence on age

Analysis of the measured PDFF in the L3 vertebra following and complementing published data by Kugel et al. [58] and Griffith et al. [59], who measured VBM fat fraction, is given in Table 4 and correspondingly plotted in Fig. 5. Table 4 tabulates the statistical differences between measured L3 bone marrow PDFF in female and male subjects grouped by age, as defined by the three studies. Differences were not significant ( $p > 0.05$ ) in any of the age groups under investigation in the present study.

### Discussion

The present study investigated cross-sectionally the dependence of VBM PDFF on age and vertebral location in children based on quantitative chemical shift-encoded water–fat imaging. The measured VBM PDFF showed a natural logarithmic increase as a function of age and a decrease from the lumbar to the cervical region in a cohort of 93 subjects. Although prior studies in adults have shown differences between males and females, the current data in children in the age range between 0 and 18 years did not readily support a sex difference.

The VBM PDFF measurements performed in the present study were based on a 3D TIMGRE sequence combined with a complex-based water–fat separation, addressing the most important confounding factors and thus enabling a robust PDFF quantification. A strong agreement between imaging-based PDFF and MRS-based PDFF was demonstrated in a subset of 37 subjects with both slope and

**Table 3** Average VBM PDFF (%) in the lumbar, thoracic and cervical spine, grouped by age and sex

Age (years)	0–0.4	0.5–1.4	1.5–2	3–4	5–8	9–18
<i>Average L5–L1</i>						
All subjects						
<i>n</i>	9	15	11	14	25	19
Mean	3.0	13.1	19.7	25.5	34.2	32.9
SD	6.9	8.4	8.4	10.0	9.2	11.3
Female						
<i>n</i>	3	7	6	6	17	10
Mean	−0.5	16.5	22.5	24	34.9	31.4
SD	4.5	8.0	7.5	8.1	9.7	13.5
Male						
<i>n</i>	6	8	5	8	8	9
Mean	4.8	10.1	16.3	26.6	32.8	34.7
SD	7.5	8.0	9.0	11.6	8.2	8.8
<i>p</i> value	0.306	0.148	0.251	0.644	0.600	0.538
<i>Average T12–T1</i>						
All subjects						
<i>n</i>	9	15	11	14	25	19
Mean	−0.5	6.8	12.8	19.7	26.3	27.2
SD	2.6	6.4	8.6	9.0	9.6	9.5
Female						
<i>n</i>	3	7	6	6	17	10
Mean	−0.1	9.0	15.0	18.4	27.0	25.8
SD	2.0	6.3	7.9	7.5	9.5	10.6
Male						
<i>n</i>	6	8	5	8	8	9
Mean	−0.6	5	10.1	20.7	24.9	28.7
SD	3.0	6.4	9.5	10.4	10.3	8.4
<i>p</i> value	0.813	0.245	0.375	0.658	0.621	0.524
<i>Average C7–C3</i>						
All subjects						
<i>n</i>	9	13	9	13	18	6
Mean	−1.6	1.5	9.1	8.8	16.0	14.9
SD	4.8	7.8	7.2	8.5	11.6	8.8
Female						
<i>n</i>	3	6	5	5	13	1
Mean	0.9	3.6	8.3	9.3	17.0	20.9
SD	1.5	4.5	5.7	6.9	12.3	0.0
Male						
<i>n</i>	6	7	4	8	5	5
Mean	−2.8	−0.3	10.1	8.5	13.4	13.7
SD	5.5	9.8	9.7	9.8	10.2	9.3
<i>p</i> value	0.305	0.393	0.738	0.869	0.574	0.521

Mean  $\pm$  SD (%) and number of the measured VBM PDFF averaged in the lumbar, thoracic and cervical spine grouped by age and sex. The *p* values reflect the likelihood of a difference between female and male subjects in the same age group and vertebral location using independent homoscedastic two-sampled *t* tests. Negative PDFF values were determined in some cases due to the usage of the magnitude discrimination approach. 109 subjects were recruited; 93 subjects were finally included; 16 cases were excluded

**Fig. 4** VBM PDFF as a function of spinal location for age groups **a** 0–0.4 years, **b** 0.5–1.4 years, **c** 1.5–2 years, **d** 3–4 years, **e** 5–8 years, and **f** 9–18 years. The equations of the linear fit (blue line,  $y = a + b \times x$ ) and  $R^2$  (numbers 1–22 were assigned to vertebrae L5–C3) are given for each age group. Outliers are indicated by red crosses. Note the increasing slope and intercept from younger towards older age groups. PDFF proton density fat fraction, VBM vertebral bone marrow

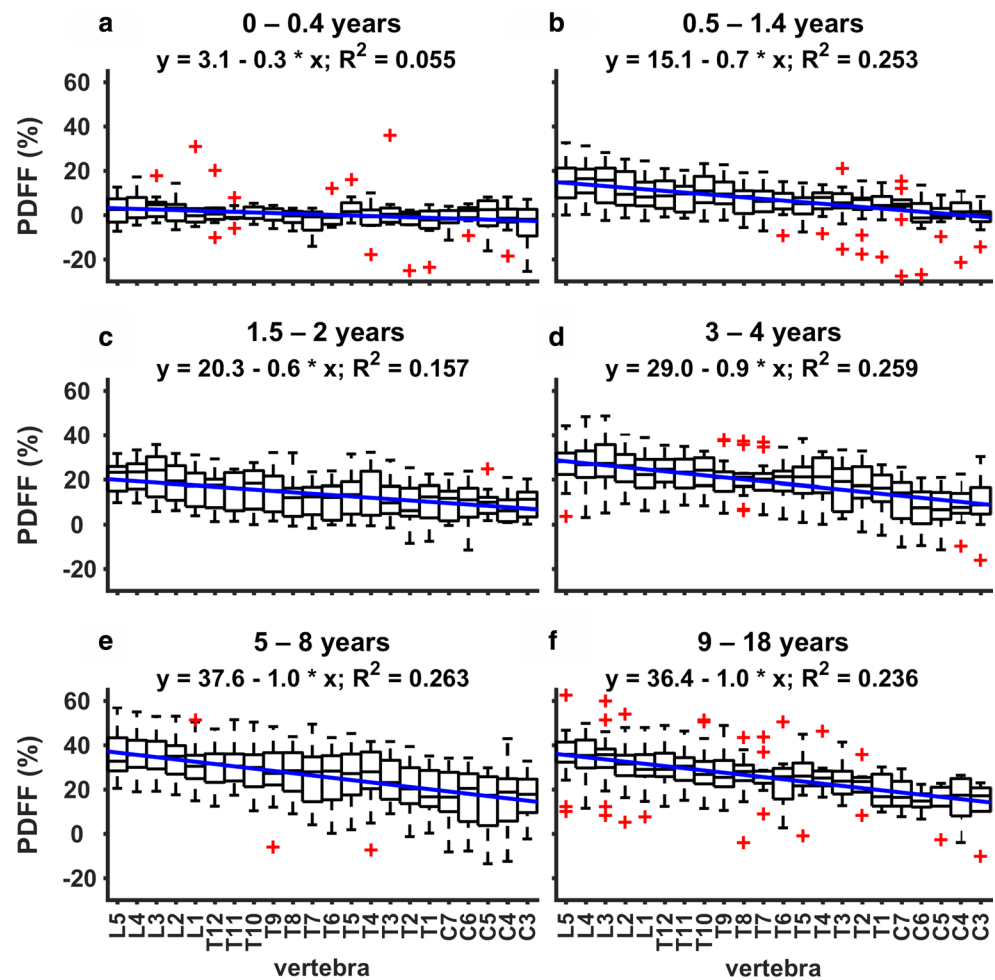


**Table 4** L3 vertebral bone marrow fat fraction (%) in different age groups

	Present study (L3)						Kugel et al.				Griffith et al.				
Age (years)	0–0.4	0.5–1.4	1.5–2	3–4	5–8	9–18	11–20	21–30	31–40	41–50	51–60	61–70	71–80	81–90	
All subjects															
<i>n</i>	9	15	11	14	25	19	15	39	42	23	17	77	121	61	
Mean	3.9	13.8	21.2	27.7	35.1	33.8	23.9	29.5	36.9	43	44.6	59.8	60.3	67.6	
SD	6.4	9.7	10.1	12.0	9.1	12.0	8.3	9.7	10.7	9.4	5.7	10.7	10.8	12.2	
Male															
<i>n</i>	6	8	5	8	8	9						28	49	37	
Mean	6.3	10.9	16.6	29.1	33.2	35.2	24.6	33.5	41.4	47.6	47.7	52.0	53.8	64.0	
SD	6.2	9.9	9.7	13.8	7.7	9.4	7.8	10.4	10.4	6.7	5.5	8.7	9.6	10.9	
Female															
<i>n</i>	3	7	6	6	17	10						49	72	24	
Mean	−0.7	17.1	25.2	25.7	36.0	32.4	23.5	27.5	29.7	37	41.8	64.2	64.7	73.2	
SD	4.5	9.2	9.5	9.9	9.7	14.4	9.0	8.8	6.3	9.3	4.6	9.1	9.2	12.2	
<i>p</i> value	0.095	0.232	0.178	0.573	0.467	0.842	0.820	0.067	<0.001	0.004	0.029	<0.001	<0.001	0.003	

Measured L3 vertebral bone marrow fat fraction (%) in age groups from 0 to 18 years (present study), 11 to 60 years (Kugel et al. [58]) and 61 to 90 years (Griffith et al. [59]). The *p*-values reflect the likelihood of a difference between female and male subjects in the bone marrow fat content in different age groups using nonparametric Mann–Whitney *U* tests (present study and Kugel et al.) or independent two-sample *t* tests (Griffith et al.).



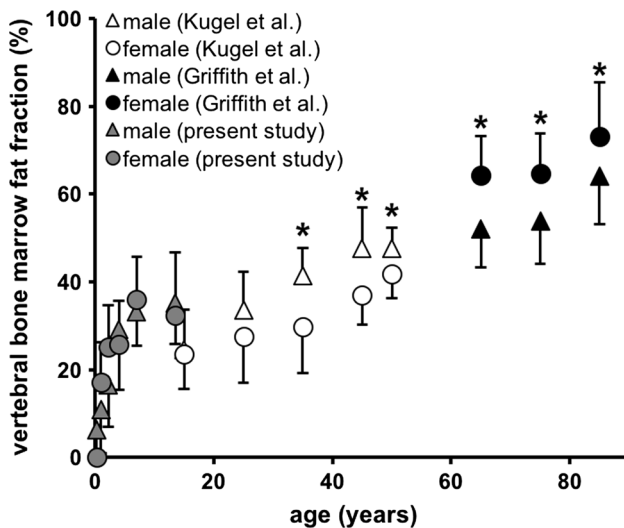


**Fig. 5** Average L3 vertebral bone marrow fat content ( $\pm$ SD indicated by *error bars*) as function of age. Statistical significant differences ( $p < 0.05$ ) between female and male vertebral bone marrow fat content are indicated by an *asterisk*. Data for age groups from 0–18, 11–60 and 61–90 years are from the current study, Kugel et al. [58] and Griffith et al. [59], respectively. *SD* standard deviation

intercept not being significantly different from 1 and 0, respectively. In some cases results showed negative imaging-based PDFF values, which is due to the employed magnitude discrimination approach [39].

Bone marrow and in particular the VBM conversion from hematopoietic to fatty marrow with age is well known and has been qualitatively well documented [2, 6]. Quantitative data on the bone marrow conversion with age, e.g. by measuring VBM PDFF, exist but are still quite limited [58, 59]. In addition, the physiology of bone marrow and how it undergoes pathologic changes is not fully understood and is still under ongoing investigations [6]. Although it has been known that only hematopoietic marrow is present at birth and that fatty marrow increases from then on with the process of aging, previous reports have assumed that the VBM fat fraction increases in infants as age advances relatively slowly [2, 60]. Instead, the present results showed that there is a very rapid increase of VBM PDFF between 0 and 2 years of age, and a relatively slower increase at 2 years and onwards. The above-mentioned rapid increase in VBM PDFF shortly after birth may imply that the conversion process is an integral part of a developmental phase. The rapid increase in VBM PDFF during the first years after birth also seems to be consistent with the appearance of VBM in  $T_1$ -weighted imaging of healthy children [61–64].

The present study investigates the VBM PDFF age dependence between 0 and 18 years, complementing the previous studies by Kugel et al. [58] and Griffith et al. [59] who investigated the age dependence of VBM fat fraction

in adults by measuring L3 vertebrae. Specifically, the present study found a logarithmic increase over age in VBM PDFF in the age groups from 0 to 18 years with insignificant ( $p > 0.05$ ) differences between female and male subjects. Kugel et al. [58] then found a further increase in VBM fat fraction for the age groups in the range from 11 to 60 years with significant sex differences for the age group 31–40 years and after showing higher VBM fat fractions in male subjects. Griffith et al. [59] investigated age groups ranging from 61 to 90 years reporting further statistically significant differences between the sexes of all age groups and a reversal of sex differences in accordance with Ishijima et al. [65]. A sharp increase in VBM fat fraction in postmenopausal women was first reported by Ishijima et al. [65], using an imaging-based approach and was later confirmed by Kugel et al. [58] and Griffith et al. [59]. This result was explained with a declining estrogen level, which, among other factors, may also cause changes in the intra-abdominal adipose tissue [66] and body fat distribution [67, 68]. At which age the sex differences exactly become significant is still speculative. Kugel et al. [58] reported that the first appearance of significant differences occurred in the age group of 31–40 years. Duda et al. [69] concluded that differences already existed at the age of 17 years (although measured in the sacrum), whereas another study [65] reported statistical significant differences in the age group of 25–54 years, and no significant differences existed in the age group of 5–24 or 55–85 years. There are also some limitations to the inter-study comparability and this might also explain the large difference of approximately 10% in the VBM fat fraction measured in the present study for the age group of 9–18 years and Kugel et al.'s [58] age group of 11–20 years. While the current study used imaging at 3T to extract PDFF, Kugel et al. [58] and Griffith et al. [59] determined a non-quantitative measure of fat fraction using Point Resolved Spectroscopy (PRESS) at 1.5T with TRs of 2000 and 3000 ms; and TEs of 40 and 25 ms, respectively. Especially  $T_2$ -weighting may be a confounding factor in the fat fraction determination in the PRESS experiments, as previously shown by Dieckmeyer et al. [16].  $T_2$  correction was not performed in the elderly population study by Griffith et al. [59] and only generally accounted for in the wide age range population study of Kugel et al. [58].

The current study also showed a decrease of the VBM PDFF measured in the region from the lumbar to the cervical vertebrae, with a slope that increased with age. Vertebral variation showing overall decreasing VBM PDFF values from the lumbar vertebrae towards the cervical vertebrae has also been previously described in preliminary studies for the lumbar vertebrae [11] and S2–T10 vertebrae [13]; in the context of osteoporosis for the L1–L4 vertebrae [70]; and in the adult population for the whole spine in an

imaging-based study published by Baum et al. [17]. However, as far as we know, the observed age dependence of the slope of the relationship between VBM PDFF and vertebral location has never been observed before.

The present study has some limitations. First, although the final patient cohort of 93 subjects involved in this study had no pathological indications that would suggest a possible impact on VBM PDFF, the use of healthy asymptomatic children would have been more ideal in establishing normative values. However, the recruitment of such a cohort would be a challenging undertaking. Second, there was only a small number of subjects in this study with more than nine years of age. Therefore, subjects older than 9 years were combined to form a single age group. A third limitation is the accuracy of using a manual segmentation method for probing the VBM compartment in a single slice, which assumes a homogeneous distribution of PDFF throughout the VBM compartment.

## Conclusion

In conclusion, the assessment of VBM PDFF in children is feasible using chemical shift-encoding based 3D TIMGRE water–fat imaging. The cohort studied here showed a sex-independent VBM PDFF of 0% shortly after birth and thereafter a natural logarithmic increase with age. The intra-individual VBM spatial variation showed a PDFF linearly decreasing from the lumbar to the cervical vertebrae, with a slope decreasing with age. Results from the present work—including the largest cohort in whom VBM PDFF development in first years of life has ever been investigated—can potentially serve as a normative database for the VBM PDFF variation with age and spinal location in children, with applications existing in the characterization of bone marrow health and physiology, and in assisting therapy planning and treatment monitoring in cases of cancer.

**Acknowledgements** We would like to thank librarian Kathy Zeblisky from Phoenix Children’s Hospital for reference assistance.

**Grant support** Stefan Ruschke was supported by the German Academic Exchange Service (DAAD) through the “Kurzstipendien für Doktorandinnen und Doktoranden” program. This work was supported by grant support from Philips Healthcare (to Dimitrios C. Karampinos). Thomas Baum received grant support from the Technical University of Munich, Faculty of Medicine (KKF H01).

## Compliance with ethical standards

**Conflict of interest** Holger Eggers is an employee of Philips Healthcare. Dimitrios Karampinos receives grant support from Philips Healthcare.

**Ethical approval** All procedures performed in studies involving human participants were in accordance with the ethical standards of the institutional and/or national research committee and with the 1964 Helsinki declaration and its later amendments or comparable ethical standards.

**Informed consent** Informed consent was obtained from all individual participants included in the study.

## References

1. Tavassoli M, Crosby WH (1970) Bone marrow histogenesis: a comparison of fatty and red marrow. *Science* 169:291–293
2. Kricun ME (1985) Red–yellow marrow conversion: its effect on the location of some solitary bone lesions. *Skelet Radiol* 14:10–19
3. Babyn PS, Ranson M, McCarville ME (1998) Normal bone marrow: signal characteristics and fatty conversion. *Magn Reson Imaging Clin N Am* 6:473–495
4. Tavassoli M (1976) Marrow adipose cells. Histochemical identification of labile and stable components. *Arch Pathol Lab Med* 100:16–18
5. Scheller EL, Doucette CR, Learman BS, Cawthorn WP, Khandaker S, Schell B, Wu B, Ding S-Y, Bredella MA, Fazeli PK, Khoury B, Jepsen KJ, Pilch PF, Klubanski A, Rosen CJ, MacDougald OA (2015) Region-specific variation in the properties of skeletal adipocytes reveals regulated and constitutive marrow adipose tissues. *Nat Commun* 6:7808
6. Scheller EL, Rosen CJ (2014) What’s the matter with MAT? marrow adipose tissue, metabolism, and skeletal health. *Ann NY Acad Sci* 1311:14–30
7. Pichardo JC, Milner RJ, Bolch WE (2011) MRI measurement of bone marrow cellularity for radiation dosimetry. *J Nucl Med* 52:1482–1489
8. MacEwan IJ, Glembotski NE, D’Lima D, Bae W, Masuda K, Rashidi HH, Mell LK, Bydder M (2014) Proton density water fraction as a biomarker of bone marrow cellularity: validation in ex vivo spine specimens. *Magn Reson Imaging* 32:1097–1101
9. Arentsen L, Yagi M, Takahashi Y, Bolan PJ, White M, Yee D, Hui S (2015) Validation of marrow fat assessment using noninvasive imaging with histologic examination of human bone samples. *Bone* 72:118–122
10. Schellinger D, Lin CS, Fertikh D, Lee JS, Lauerman WC, Henderson F, Davis B (2000) Normal lumbar vertebrae: anatomic, age, and sex variance in subjects at proton MR spectroscopy-initial experience. *Radiology* 215:910–916
11. Liney GP, Bernard CP, Manton DJ, Turnbull LW, Langton CM (2007) Age, gender, and skeletal variation in bone marrow composition: a preliminary study at 3.0T. *J Magn Reson Imaging* 26:787–793
12. Roldan-Valadez E, Piña-Jimenez C, Favila R, Rios C (2013) Gender and age groups interactions in the quantification of bone marrow fat content in lumbar spine using 3T MR spectroscopy: a multivariate analysis of covariance (Mancova). *Eur J Radiol* 82:e697–e702
13. Martin J, Nicholson G, Cowin G, Ilente C, Wong W, Kennedy D (2014) Rapid determination of vertebral fat fraction over a large range of vertebral bodies. *J Med Imaging Radiat Oncol* 58:155–163
14. Bredella MA, Daley SM, Kalra MK, Brown JK, Miller KK, Torriani M (2015) Marrow adipose tissue quantification of the

- lumbar spine by using dual-energy CT and single-voxel 1H MR spectroscopy: a feasibility study. *Radiology* 277:230–235
15. Barber QM, Yahya A (2015) Aspects of spinal bone marrow fat to water quantification with magnetic resonance spectroscopy at 3T. *Biomed Phys Eng Express* 1:047001
  16. Dieckmeyer M, Ruschke S, Cordes C, Yap SP, Kooijman H, Hauner H, Rummeny EJ, Bauer JS, Baum T, Karampinos DC (2015) The need for T2 correction on MRS-based vertebral bone marrow fat quantification: implications for bone marrow fat fraction age dependence. *NMR Biomed* 28:432–439
  17. Baum T, Yap SP, Dieckmeyer M, Ruschke S, Eggers H, Kooijman H, Rummeny EJ, Bauer JS, Karampinos DC (2015) Assessment of whole spine vertebral bone marrow fat using chemical shift-encoding based water-fat MRI. *J Magn Reson Imaging* 42:1018–1023
  18. Kühn J-P, Hernando D, Meffert PJ, Reeder S, Hosten N, Laqua R, Steveling A, Ender S, Schröder H, Pillich D-T (2013) Proton-density fat fraction and simultaneous R2\* estimation as an MRI tool for assessment of osteoporosis. *Eur Radiol* 23:3432–3439
  19. Karampinos DC, Ruschke S, Dieckmeyer M, Eggers H, Kooijman H, Rummeny EJ, Bauer JS, Baum T (2015) Modeling of T2\* decay in vertebral bone marrow fat quantification. *NMR Biomed* 28:1535–1542
  20. Schellinger D, Lin CS, Hatipoglu HG, Fertikh D (2001) Potential value of vertebral proton MR spectroscopy in determining bone weakness. *AJNR Am J Neuroradiol* 22:1627
  21. Griffith JF, Yeung DKW, Antonio GE, Wong SYS, Kwok TCY, Woo J, Leung PC (2006) Vertebral marrow fat content and diffusion and perfusion indexes in women with varying bone density: MR evaluation. *Radiology* 241:831–838
  22. Karampinos DC, Ruschke S, Gordijenko O, Grande Garcia E, Kooijman H, Burgkart R, Rummeny EJ, Bauer JS, Baum T (2015) Association of MRS-based vertebral bone marrow fat fraction with bone strength in a human in vitro model. *J Osteoporos* 2015:1–8
  23. Bredella MA, Torriani M, Ghomi RH, Thomas BJ, Brick DJ, Gerweck AV, Rosen CJ, Klibanski A, Miller KK (2011) Vertebral bone marrow fat is positively associated with visceral fat and inversely associated with IGF-1 in obese women. *Obesity (Silver Spring)* 19:49–53
  24. Bredella MA, Gill CM, Gerweck AV, Landa MG, Kumar V, Daley SM, Torriani M, Miller KK (2013) Ectopic and serum lipid levels are positively associated with bone marrow fat in obesity. *Radiology* 269:534–541
  25. Cordes C, Dieckmeyer M, Ott B, Shen J, Ruschke S, Settles M, Eichhorn C, Bauer JS, Kooijman H, Rummeny EJ, Skurk T, Baum T, Hauner H, Karampinos DC (2015) MR-detected changes in liver fat, abdominal fat, and vertebral bone marrow fat after a four-week calorie restriction in obese women. *J Magn Reson Imaging* 42:1272–1280
  26. Kim YP, Kannengiesser S, Paek M-Y, Kim S, Chung T-S, Yoo YH, Yoon C-S, Song H-T, Lee YH, Suh J-S (2014) Differentiation between focal malignant marrow-replacing lesions and benign red marrow deposition of the spine with T2\*-corrected fat-signal fraction map using a three-echo volume interpolated breath-hold gradient echo Dixon sequence. *Korean J Radiol* 15:781–791
  27. Schraml C, Schmid M, Gatidis S, Schmidt H, la Fougère C, Nikolaou K, Schwenzler NF (2015) Multiparametric analysis of bone marrow in cancer patients using simultaneous PET/MR imaging: correlation of fat fraction, diffusivity, metabolic activity, and anthropometric data. *J Magn Reson Imaging* 42:1048–1056
  28. Ollivier L, Brisse H, Leclère J (2015) Bone marrow imaging: follow-up after treatment in cancer patients. *Cancer Imaging* 2:90–92
  29. Daldrop-Link HE, Henning T, Link TM (2007) MR imaging of therapy-induced changes of bone marrow. *Eur Radiol* 17:743–761
  30. Bolan PJ, Arentsen L, Sueblinvong T, Zhang Y, Moeller S, Carter JS, Downs LS, Ghebre R, Yee D, Froelich J, Hui S (2013) Water-fat MRI for assessing changes in bone marrow composition due to radiation and chemotherapy in gynecologic cancer patients. *J Magn Reson Imaging* 38:1578–1584
  31. Carmona R, Pritz J, Bydder M, Gulaya S, Zhu H, Williamson CW, Welch CS, Vaida F, Bydder G, Mell LK (2014) Fat composition changes in bone marrow during chemotherapy and radiation therapy. *Int J Radiat Oncol Biol Phys* 90:155–163
  32. Cristy M (1981) Active bone marrow distribution as a function of age in humans. *Phys Med Biol* 26:389–400
  33. Mouloupoulos LA, Dimopoulos MA (1997) Magnetic resonance imaging of the bone marrow in hematologic malignancies. *Blood* 90:2127–2147
  34. Glover GH, Schneider E (1991) Three-point dixon technique for true water/fat decomposition with B0 inhomogeneity correction. *Magn Reson Med* 18:371–383
  35. Hernando D, Haldar JP, Sutton BP, Ma J, Kellman P, Liang ZP (2008) Joint estimation of water/fat images and field inhomogeneity map. *Magn Reson Med* 59:571–580
  36. Yu H, Yu H, McKenzie CA, Shimakawa A, Shimakawa A, Vu AT, Brau ACS, Beatty PJ, Pineda AR, Brittain JH, Brittain JH, Reeder SB, Reeder SB (2007) Multiecho reconstruction for simultaneous water-fat decomposition and T2\* estimation. *J Magn Reson Imaging* 26:1153–1161
  37. Bydder M, Yokoo T, Hamilton G, Middleton MS, Chavez AD, Schwimmer JB, Lavine JE, Sirlin CB (2008) Relaxation effects in the quantification of fat using gradient echo imaging. *Magn Reson Imaging* 26:347–359
  38. Yu H, Shimakawa A, McKenzie CA, Brodsky E, Brittain JH, Reeder SB (2008) Multiecho water-fat separation and simultaneous R2\* estimation with multifrequency fat spectrum modeling. *Magn Reson Med* 60:1122–1134
  39. Liu C-Y, McKenzie CA, Yu H, Brittain JH, Reeder SB (2007) Fat quantification with IDEAL gradient echo imaging: correction of bias from T1 and noise. *Magn Reson Med* 58:354–364
  40. Karampinos DC, Yu H, Yu H, Shimakawa A, Shimakawa A, Link TM, Majumdar S (2011) T1-corrected fat quantification using chemical shift-based water/fat separation: application to skeletal muscle. *Magn Reson Med* 66:1312–1326
  41. Karampinos DC, Yu H, Shimakawa A, Link TM, Majumdar S (2012) Chemical shift-based water/fat separation in the presence of susceptibility-induced fat resonance shift. *Magn Reson Med* 68:1495–1505
  42. Hernando D, Sharma SD, Kramer H, Reeder SB (2014) On the confounding effect of temperature on chemical shift-encoded fat quantification. *Magn Reson Med* 72:464–470
  43. Colgan TJ, Hernando D, Sharma SD, Reeder SB (2016) The effects of concomitant gradients on chemical shift encoded MRI. *Magn Reson Med*. doi:10.1002/mrm.26461
  44. Ruschke S, Eggers H, Kooijman H, Diefenbach MN, Baum T, Haase A, Rummeny EJ, Hu HH, Karampinos DC (2016) Correction of phase errors in quantitative water-fat imaging using a monopolar time-interleaved multi-echo gradient echo sequence. *Magn Reson Med*. doi:10.1002/mrm.26485
  45. Lu W, Yu H, Shimakawa A, Alley M, Reeder SB, Hargreaves BA (2008) Water-fat separation with bipolar multiecho sequences. *Magn Reson Med* 60:198–209
  46. Yu H, Shimakawa A, McKenzie CA, Lu W, Reeder SB, Hinks RS, Brittain JH (2010) Phase and amplitude correction for multi-echo water-fat separation with bipolar acquisitions. *J Magn Reson Imaging* 31:1264–1271
  47. Yu H, Shimakawa A, Hines CDG, McKenzie CA, Hamilton G, Sirlin CB, Brittain JH, Reeder SB (2011) Combination of

- complex-based and magnitude-based multiecho water–fat separation for accurate quantification of fat-fraction. *Magn Reson Med* 66:199–206
48. Hernando D, Hines CDG, Yu H, Reeder SB (2012) Addressing phase errors in fat–water imaging using a mixed magnitude/complex fitting method. *Magn Reson Med* 67:638–644
  49. Peterson P, Mansson S (2014) Fat quantification using multi-echo sequences with bipolar gradients: investigation of accuracy and noise performance. *Magn Reson Med* 71:219–229
  50. Fazeli PK, Horowitz MC, MacDougald OA, Scheller EL, Rodeheffer MS, Rosen CJ, Klibanski A (2013) Marrow fat and bone—new perspectives. *J Clin Endocrinol Metab* 98:935–945
  51. Rosen CJ, Ackert-Bicknell C, Rodriguez JP, Pino AM (2009) Marrow fat and the bone microenvironment: developmental, functional, and pathological implications. *Crit Rev Eukaryot Gene Expr* 19:109–124
  52. Pineda AR, Reeder SB, Wen Z, Pelc NJ (2005) Cramér-Rao bounds for three-point decomposition of water and fat. *Magn Reson Med* 54:625–635
  53. Gee CS, Nguyen JTK, Marquez CJ, Heunis J, Lai A, Wyatt C, Han M, Kazakia G, Burghardt AJ, Karampinos DC, Carballido-Gamio J, Krug R (2015) Validation of bone marrow fat quantification in the presence of trabecular bone using MRI. *J Magn Reson Imaging* 42:539–544
  54. Berglund J, Johansson L, Ahlström H, Kullberg J (2010) Three-point Dixon method enables whole-body water and fat imaging of obese subjects. *Magn Reson Med* 63:1659–1668
  55. Hu HH, Börnert P, Hernando D, Kellman P, Ma J, Jingfei Reeder S, Sirlin C (2012) ISMRM workshop on fat–water separation: insights, applications and progress in MRI. *Magn Reson Med* 68:378–388
  56. Ren J, Dimitrov I, Sherry AD, Malloy CR (2008) Composition of adipose tissue and marrow fat in humans by <sup>1</sup>H NMR at 7T. *J Lipid Res* 49:2055–2062
  57. Bydder M, Girard O, Hamilton G, Hamilton G (2011) Mapping the double bonds in triglycerides. *Magn Reson Imaging* 29:1041–1046
  58. Kugel H, Jung C, Schulte O, Heindel W (2001) Age- and sex-specific differences in the <sup>1</sup>H-spectrum of vertebral bone marrow. *J Magn Reson Imaging* 13:263–268
  59. Griffith JF, Yeung DKW, Ma HT, Leung JCS, Kwok TCY, Leung PC (2012) Bone marrow fat content in the elderly: a reversal of sex difference seen in younger subjects. *J Magn Reson Imaging* 36:225–230
  60. Custer RP (1932) Studies on the structure and function of bone marrow. 17:951–960
  61. Walker HS, Dietrich RB, Flannigan BD, Lufkin RB, Peacock WJ, Kangaroo H (1987) Magnetic resonance imaging of the pediatric spine. *Radiographics* 7:1129–1152
  62. Sebag GH, Dubois J, Tabet M, Bonato A, Lallemand D (1993) Pediatric spinal bone marrow: assessment of normal age-related changes in the MRI appearance. *Pediatr Radiol* 23:515–518
  63. Taccone A, Oddone M, Occhi M, Dell’Acqua A, Ciccone MA (1995) MRI “road-map” of normal age-related bone marrow. *Pediatr Radiol* 25:588–595
  64. Foster K, Chapman S, Johnson K (2004) MRI of the marrow in the paediatric skeleton. *Clin Radiol* 59:651–673
  65. Ishijima H, Ishizaka H, Horikoshi H, Sakurai M (1996) Water fraction of lumbar vertebral bone marrow estimated from chemical shift misregistration on MR imaging: normal variations with age and sex. *AJR Am J Roentgenol* 167:355–358
  66. Gower BA, Nagy TR, Goran MI, Toth MJ (1998) Fat distribution and plasma lipid-lipoprotein concentrations in pre- and postmenopausal women. *J Obes* 22:605–611
  67. Toth MJ, Tchernof A, Sites CK, Poehlman ET (2000) Menopause-related changes in body fat distribution. *Ann NY Acad Sci* 904:502–506
  68. Blouin K, Boivin A, Tchernof A (2008) Androgens and body fat distribution. *J Steroid Biochem Mol Biol* 108:272–280
  69. Duda SH, Laniado M, Schick F, Strayle M, Claussen CD (1995) Normal bone marrow in the sacrum of young adults: differences between the sexes seen on chemical-shift MR imaging. *AJR Am J Roentgenol* 164:935–940
  70. Li X, Kuo D, Schafer AL, Porzig A, Link TM, Black D, Schwartz AV (2011) Quantification of vertebral bone marrow fat content using 3 tesla MR spectroscopy: reproducibility, vertebral variation, and applications in osteoporosis. *J Magn Reson Imaging* 33:974–979